Nanoscale

PAPER

View Article Online
View Journal | View Issue

Cite this: *Nanoscale*, 2017, **9**, 14215

Analytical, numerical, and experimental studies of viscoelastic effects on the performance of soft piezoelectric nanocomposites†

Jing Li,[a,b,c] Zhiren Zhu,[d] Lichen Fang,[a,b] Shu Guo,[d] Ugur Erturun,[e] Zeyu Zhu,[a,b] James E. West,[e] Somnath Ghosh[a,b,d] and Sung Hoon Kang *[a,b]

Piezoelectric composite (p-NC) made of a polymeric matrix and piezoelectric nanoparticles with conductive additives is an attractive material for many applications. As the matrix of p-NC is made of viscoelastic materials, both elastic and viscous characteristics of the matrix are expected to contribute to the piezoelectric response of p-NC. However, there is limited understanding of how viscoelasticity influences the piezoelectric performance of p-NC. Here we combined analytical and numerical analyses with experimental studies to investigate effects of viscoelasticity on piezoelectric performance of p-NC. The viscoelastic properties of synthesized p-NCs were controlled by changing the ratio between monomer and cross-linker of the polymer matrix. We found good agreement between our analytical models and experimental results for both quasi-static and dynamic loadings. It is found that, under quasi-static loading conditions, the piezoelectric coefficients (d_{33}) of the specimen with the lowest Young's modulus (~0.45 MPa at 5% strain) were ~120 pC N^{-1}, while the one with the highest Young's modulus (~1.3 MPa at 5% strain) were ~62 pC N^{-1}. The results suggest that softer matrices enhance the energy harvesting performance because they can result in larger deformation for a given load. Moreover, from our theoretical analysis and experiments under dynamic loading conditions, we found the viscous modulus of a matrix is also important for piezoelectric performance. For instance, at 40 Hz and 50 Hz the storage moduli of the softest specimen were ~0.625 MPa and ~0.485 MPa, while the loss moduli were ~0.108 MPa and ~0.151 MPa, respectively. As piezocomposites with less viscous loss can transfer mechanical energy to piezoelectric particles more efficiently, the dynamic piezoelectric coefficient (d'_{33}) measured at 40 Hz (~53 pC N^{-1}) was larger than that at 50 Hz (~47 pC N^{-1}) though it has a larger storage modulus. As an application of our findings, we fabricated 3D piezo-shells with different viscoelastic properties and compared the charging time. The results showed a good agreement with the predicted trend that the composition with the smallest elastic and viscous moduli showed the fastest charging rate. Our findings can open new opportunities for optimizing the performance of polymer-based multifunctional materials by harnessing viscoelasticity.

Received 15th July 2017,
Accepted 8th September 2017

DOI: 10.1039/c7nr05163h

rsc.li/nanoscale

Introduction

The development trend of portable and wearable electronics results in a pressing need for harvesting sustainable energy from ambient environment to power devices.[1] Compared to large-scale outdoor renewable energy sources, such as water wave,[2] wind energy,[3] and solar energy,[4] mechanical energy is easily accessible for driving small electronics. Therefore, there has been growing interest in the use of nanogenerators[5–7] for sustainable and portable power applications by harvesting mechanical energy. Active research has been conducted to utilize devices made of piezoelectric materials as power sources for wearable electronics,[8,9] healthcare devices,[10,11] and self-powered sensors[12,13] by harvesting energy from ambient vibration or physical activities. For example, Wang and co-

[a]*Department of Mechanical Engineering, Johns Hopkins University, Baltimore, MD 21218, USA. E-mail: shkang@jhu.edu*
[b]*Hopkins Extreme Materials Institute, Johns Hopkins University, Baltimore, MD 21218, USA*
[c]*Hubei Key Laboratory of Advanced Technology for Automotive Components, Wuhan University of Technology, Wuhan, Hubei 430070, PR China*
[d]*Department of Civil Engineering, Johns Hopkins University, Baltimore, MD 21218, USA*
[e]*Department of Electrical & Computer Engineering, Johns Hopkins University, Baltimore, MD 21218, USA*

†Electronic supplementary information (ESI) available. See DOI: 10.1039/c7nr05163h

workers have developed the first nanogenerator based on piezoelectric ZnO nanowires for energy harvesting.[8,14–16] In addition, perovskite-structured ceramics, such as lead zirconate titanate ($Pb[Zr_xTi_{1-x}]O_3$) and barium titanate ($BaTiO_3$, BTO thereafter), have been used for its high piezoelectric conversion efficiency while they are brittle thus allow very limited deformation before failure.[19–21] Besides ceramics, piezoelectric polymers, such as poly(vinylidene fluoride) (PVDF), also have been used for energy harvesting due to their good piezoelectric properties and mechanical stabilities[9,17,18] while they have limitations in shape formation and allowable strains.

Beyond aforementioned materials, polymer-based piezoelectric nanocomposite (p-NC) made of a polymeric matrix and piezoelectric nanoparticles with a small amount of conductive additives[22–28] is a new class of material that enables use of piezoelectricity in a broad range of applications due to its good conversion efficiency, flexibility in shape formation, and accommodation of large deformation. To improve the energy generation capability of p-NC, previous studies determined the composition of the piezocomposites by measuring electric outputs as they varied the ratio among the constituents of composites.[22,29,30] There have been also efforts to further enhance the properties of piezocomposites by aligning the filler piezoelectric particles,[31] modifying particle shapes[32] or controlling the porosity.[33] In addition, there were also empirical studies to measure the effects of the polymer matrix on piezoelectric properties.[34] However, there is no quantitative understanding between the viscoelastic properties of the composites and their piezoelectric properties.

We are inspired by the fact that the matrix that consists of the major portion of piezoelectric composites is made of viscoelastic materials. In contrast to the elastic materials that store all energy upon external forces and release the stored energy with the removal of the forces, viscoelastic materials lose a part of the energy during a loading-unloading cycle. As shown in Fig. 1a, the p-NC with viscoelastic matrix can be described as combination of elastic and viscous parts. During the deformation process of a viscoelastic body, part of the total work of deformation is dissipated as heat through viscous loss, which reduces the resulting piezoelectric outputs, because mechanical energy is expected to be efficiently transferred to piezoelectric particles through the matrix. Then, the remaining energy, which is stored as elastic strain energy, can be converted to electrical energy. Therefore, both elastic and viscous parts of the viscoelastic piezocomposite play important roles in the resulting piezoelectric outputs. Thus, the energy harvesting performance can be further enhanced by optimizing the viscoelastic properties of the composite for the efficient transfer of mechanical energy to the active piezoelectric material.

Here, we report analytical, numerical, and experimental studies to systematically investigate the effects of viscoelasticity on the piezoelectric performance of soft piezoelectric nanocomposite (p-NC) under both quasi-static and dynamic loading conditions. We first derive analytical expressions that consider small viscoelastic deformation of the p-NC. Then, we validate the analytical model with experiments by synthesizing and testing p-NCs with different viscoelastic properties. We also use experimentally validated numerical models to systematically investigate effects of different material parameters and to predict the evolution of electric field under dynamic loading conditions. The numerical model can help us to find an optimal set of material parameters in p-NCs for best piezoelectric performance. As potential applications of the findings, we fabricate 3D shell piezoelectric structures using p-NCs with different viscoelastic properties to charge a commercial capacitor and compare the charging rates to demonstrate the piezoelectric performance of the p-NC with different viscoelastic properties.

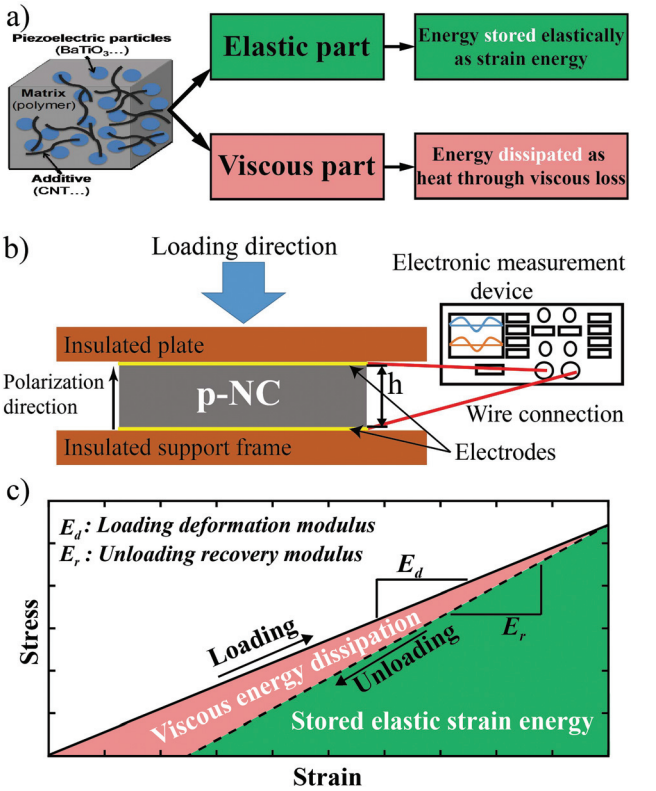

Fig. 1 Schematic illustrations of (a) a viscoelastic piezoelectric nanocomposite consists of both elastic part and viscous part, which can store energy through elastic deformation and dissipate energy through viscous loss, respectively, (b) the theoretical analysis setting for a measured piezoelectric response of a p-NC under compression, and (c) the energy storage and dissipation during the deformation process from the loading loop of a viscoelastic material.

Analytic studies

An analytic model coupling the piezoelectric behavior and the small viscoelastic deformation of the p-NC is developed from energy conservation during energy conversion. The setting for theoretical analysis of piezoelectric response of a p-NC under compression is shown in Fig. 1b. The p-NC is sandwiched between two flat plates and the loading direction is parallel to the polarization direction. The piezoelectric responses are monitored by the connected electronics.

We assumed that p-NCs have constant volume under loading and the stored deformation energy is uniformly distributed within the p-NC by approximating that the conductive nanoparticles have negligible contributions to the stress distribution within the p-NC. As demonstrated in Fig. 1a, during the deformation process of a viscoelastic p-NC, a part of the total work of deformation is dissipated as heat through viscous loss, while the remainder energy is stored as elastic strain energy, which can be converted to electrical energy. Therefore, the effective mechanical energy applied to the piezoelectric particles (W_{piezo}) can be calculated as eqn (1):

$$W_{piezo} = V_{piezo}(U_S - U_D) \quad (1)$$

where V_{piezo} is the volume of piezoelectric particles, U_S and U_D are the stored deformation energy density (energy/volume) and viscously dissipated energy density, respectively. The p-NC is assumed to be transversely isotropic with a polarization direction normal to the surface. The electrical energy density (U_E) can be described as $U_E = \varepsilon_{piezo}|\boldsymbol{E}|^2/2$ (ε_{piezo}: permittivity of piezoelectric particles, $\boldsymbol{E}$: electric field vector).[35] When electric charges are generated by the piezoelectric particles, the electric potential energy (W_E) among the p-NC can be described as eqn (2):

$$W_E = VU_E = V\varepsilon_{piezo}|\boldsymbol{E}|^2/2 \quad (2)$$

where V is the volume of the p-NC.

Because the electric potential energy is generated from the mechanical energy applied to the piezoelectric particles, we assume that the effective mechanical energy applied to the piezoelectric particles (W_{piezo}) is equal to the converted electrical energy (W_E). Therefore, by combining eqn (1) and (2), the magnitude of electric field vector ($\boldsymbol{E}$) can be written as eqn (3):

$$|\boldsymbol{E}| = \sqrt{\frac{2V_{piezo}(U_S - U_D)}{\varepsilon_{piezo}V}} \quad (3)$$

Piezoelectric coefficient (d_{ij}) is used to quantify the direct piezoelectric effect, and it's expressed as $d_{ij} = D_i/\sigma_j$ (D_i is the electric displacement and σ_j is the applied stress).[36] The subscripts "i" and "j" indicate the directions of the induced electrical field and the mechanical loading, respectively. For example, d_{33} is for the situation when the electric field and the mechanical loading are both along the polarization axis ("3" direction). Here E_3 is the only nonzero component in electric field vector ($\boldsymbol{E}$), so $E_3 = |\boldsymbol{E}|$. Then, according to the definition of electric displacement, we have $D_3 = \varepsilon_{p\text{-}NC}E_3 = \varepsilon_{p\text{-}NC}|\boldsymbol{E}|$,[37] where $\varepsilon_{p\text{-}NC}$ is the permittivity of the p-NC. By combining with eqn (3), the piezoelectric constant in the polarization direction (d_{33}) can be described as eqn (4):

$$d_{33} = \frac{D_3}{\sigma_3} = \frac{\varepsilon_{p\text{-}NC}}{\sigma_3}\sqrt{\frac{2V_{piezo}(U_S - U_D)}{\varepsilon_{piezo}V}} \quad (4)$$

Additionally, the energy storage and dissipation can be quantified from the hysteretic stress–strain curve as the area of the loop being equal to the energy lost during the loading-unloading cycle.[38] Fig. 1c shows the schematic of the energy storage and dissipation during the deformation process from a cyclic loading loop of a viscoelastic material. In the figure, the pink area indicates the dissipated energy during the loading/unloading cycle through viscous losses. The green area indicates the stored strain energy, which can be transferred to piezoelectric particles for generating electrical output.

Here, the p-NC is assumed to be a linear viscoelastic material and the loading/unloading moduli were kept constant at small deformation. Thus, under the quasi-static loading condition, the stored deformation energy density (U_S) and viscously dissipated energy density (U_D) of the composite material system can be obtained from the loading deformation/unloading recovery moduli, given as (see ESI S1† for the derivation details) eqn (5) and (6):

$$U_S = \frac{1}{2}E_d\varepsilon^2 \quad (5)$$

$$U_D = \frac{1}{2}\left(\frac{1}{E_d} - \frac{1}{E_r}\right)\sigma^2 \quad (6)$$

where E_d and E_r are the loading deformation modulus and unloading recovery modulus, respectively; σ is the applied stress and ε is the strain. Then, by substituting eqn (5) and (6) into eqn (4), the piezoelectric coefficient of the p-NC in the polarization direction (d_{33}) can be written as eqn (7) under quasi-static loading condition (see ESI S1† for the derivation details):

$$d_{33} = \varepsilon_{p\text{-}NC}\sqrt{\frac{V_{piezo}}{VE_r\varepsilon_{piezo}}} \quad (7)$$

where $\varepsilon_{p\text{-}NC}$ is the permittivity of the p-NC, V_{piezo} is the volume of piezoelectric particles, V is the volume of the p-NC, ε_{piezo} is the permittivity of piezoelectric particles. The eqn (7) suggests that the piezoelectric coefficient (d_{33}) is related to the volume fraction of piezoelectric fillers and the permittivity of the p-NC as well as the viscoelastic unloading recovery modulus (E_r) of the p-NC.

On the other hand, it is known that viscoelastic materials have elements of viscous properties and exhibit time-dependent strain. The mechanical properties will change as a function of the loading frequency under the dynamic loading conditions. Therefore, to further explore the viscoelastic influence on the piezoelectric response, we conducted dynamic analysis. Mathematically, to determine the stress and strain relation of the viscoelastic materials, elasticity and viscosity terms can be modeled as linear combinations of spring(s) and dashpot(s), respectively. Energy is stored in the spring(s) while it is dissipated in the dashpot(s). The eqn (8) and (9) show the energy storage ($U_S(t)$) and dissipation ($U_D(t)$)[39] based on spring and dashpot models.

$$U_S(t) = \frac{1}{2}\sum_n G_n{\varepsilon_{sn}}^2(t) = \frac{1}{2}\sum_n J_n{\sigma_{sn}}^2(t) \quad (8)$$

$$U_D(t) = \sum_n \eta_n{\dot{\varepsilon}_{dn}}^2(t) = \sum_n \phi_n{\sigma_{dn}}^2(t) \quad (9)$$

where G_n is the elastic modulus of the n^{th} spring, J_n is its compliance, ε_{sn} and σ_{sn} are the strain and stress of the n^{th} spring,

respectively, η_n is the coefficient of viscosity of the n^{th} dashpot and φ_n is its coefficient of fluidity, $\dot{\varepsilon}_{dn}$ is the rate of strain, and σ_{dn} is the stress of the n^{th} dashpot.

Here, to simplify these equations, the Maxwell model[39,40] is used, which presents the system with a purely viscous damper and a purely elastic spring connected in series, and the viscoelasticity is described by dynamic modulus (G) that consists of storage modulus (G') and loss modulus (G''). G' and G'' are used to define the energy stored in a specimen due to the applied strain and the dissipation of energy, respectively. At the point of the maximum strain, the stored energy per unit volume in the spring of the Maxwell unit in response to the sinusoidal strain excitation is given by eqn (10):

$$U_S = (\varepsilon^2/2)G' \tag{10}$$

The energy dissipated per unit volume over any quarter cycle of the excitation in the dashpot of the Maxwell unit can be written as eqn (11):

$$U_D = (\pi\varepsilon^2/4)G'' \tag{11}$$

By combining the eqn (4), (10) and (11), the piezoelectric constant (d'_{33}) under dynamic loading conditions can be described as eqn (12).

$$d'_{33} = \frac{\varepsilon_{p\text{-}NC}}{\sigma}\sqrt{\frac{2V_{piezo}((\varepsilon^2/2)G' - (\pi\varepsilon^2/4)G'')}{\varepsilon_{piezo}V}} \tag{12}$$

where strain, $\varepsilon = \sigma/G$ and dynamic modulus, $G = \sqrt{G'^2 + G''^2}$. Therefore, the eqn (12) can be written as eqn (13):

$$d'_{33} = \frac{\varepsilon_{p\text{-}NC}}{\sqrt{G'^2 + G''^2}}\sqrt{\frac{2V_{piezo}((1/2)G' - (\pi/4)G'')}{\varepsilon_{piezo}V}} \tag{13}$$

From the eqn (13), the dynamic piezoelectric coefficient (d'_{33}) is related to the volume fraction of piezoelectric fillers and the permittivity of the p-NC. This is same as the quasi-static case, while both storage and loss moduli of the composite will contribute to the resulting piezoelectric outputs.

Since the polymeric matrix is nearly incompressible, it is also worthwhile to note the effect of incompressibility on piezoelectric behaviors. Consider a perfectly incompressible material ($\nu = 0.5$) poled to have a piezoelectric coefficient d_{33}. This results in the non-zero piezoelectric stress coefficients $e_{31} = e_{32} = \lambda d_{33}$ and $e_{33} = (\lambda + 2\mu)d_{33}$, where $\lambda = \frac{E\nu}{(1+\nu)(1-2\nu)}$ and $\mu = \frac{E}{2(1+\nu)}$ are the Lamé constants. Note that the piezoelectric stress coefficient is defined as $e_{mnp} = d_{mjk}C_{jknp}$, where d_{mjk} is the piezoelectric (strain) coefficient discussed earlier and C_{jknp} is the elasticity stiffness tensor. From this, we can deduce $e_{31}/e_{33} = \nu/(1-\nu)$, and when $\nu = 0.5$, $e_{31} = e_{32} = e_{33}$. In other words, the piezoelectric contribution from a unit principal strain in the loading direction and that from a unit principal strain in the transverse direction are equal in an incompressible material. In the case of pure tension or compression, the Green-Lagrange strain tensor has the non-zero components $E_{11} = E_{22} = (1/\alpha - 1)/2$ and $E_{33} = (\alpha^2 - 1)/2$, where $\alpha = \alpha_3$ is the principal stretch along the loading direction.[41–43] It can be seen that $E_{11} + E_{22} + E_{33} \geq 0$ always holds, with $E_{11} + E_{22} + E_{33} = 0$ satisfied only at $\alpha = 1$, *i.e.* no deformation. For a perfectly incompressible material, we thus expect the generated electric field to be always in the same direction when the material is subjected to uniaxial tension and compression.

Experimental validations

We have conducted experimental studies to verify the theoretical analysis in the previous section. We synthesized piezoelectric nanocomposites (p-NC) with different viscoelastic properties based on polydimethylsiloxane (PDMS) (Sylgard 184 from Dow Corning) matrix, $BaTiO_3$ nanoparticles (BTO NPs) (available from US Research Nanomaterials, Inc.), and multi-walled carbon nanotubes (CNTs) (available from US Research Nanomaterials, Inc.) conductive additives. For synthesis, multi-walled CNTs and BTO NPs were added to uncured PDMS. After stirring by planetary revolutionary mixer (KK-400W, Mazerustar) for 270 seconds, the mixture was set to cure. The viscoelastic properties of the p-NCs were controlled by changing the ratio between monomer and cross-linker of the PDMS matrix.[44,45] The mixing ratios (λ) between PDMS monomor and curing agent were 5 : 1, 10 : 1 and 20 : 1 by weight, respectively. After curing, Au/Cr electrodes were deposited on top and bottom sides of the p-NCs using sputtering deposition. The detailed sample preparation procedures are described in the Experimental section and the schematic diagrams of the fabrication process of the p-NC are shown in Fig. S1 in ESI.† After electrode deposition, we conducted a poling process to align dipoles because dipoles are randomly aligned in as-synthesized piezocomposites.[46] The polarization process of the p-NCs is conducted at 100 kV cm^{-1}, 140 °C for 30 minutes (see ESI S5† for details).

For the characterization of viscoelastic properties of the p-NCs, we firstly conducted uniaxial quasi-static loading and unloading tests followed by cyclic loading tests on specimens with the matrix mixing ratio λ = 5 : 1, 10 : 1, and 20 : 1 by MTS Insight 5 electromechanical test system. From the quasi-static tensile tests, all samples exhibited elastomer-type behaviors,[47] while the elastic modulus of p-NCs with different mixing ratios showed the same trend as pure PDMS with different mixing ratios (see ESI S3†). Within the measurement results, we also note that all p-NCs have good ductility with a high tensile strain beyond 100%, which is essential for stretchable self-powered device applications.[7]

Under quasi-static loading condition, the mechanical energy storage and dissipation can be quantified by the hysteresis loop in the cyclic loading stress–strain curve.[38] Therefore, we conducted cyclic loading-unloading tensile tests of the p-NCs at different strain values (ε = 5%, 10%, and 20% at a strain rate of 0.005 s^{-1}) (see ESI S4† for details). The loading deformation moduli (E_d) of 5 : 1, 10 : 1 and 20 : 1 p-NC are

1.32 ± 0.044 MPa, 1.72 ± 0.082 MPa, and 0.45 ± 0.023 MPa at ε = 5% while the unloading recovery moduli (E_r) are 1.45 ± 0.075 MPa, 1.85 ± 0.112 MPa and 0.52 ± 0.031 MPa, respectively, as shown in Fig. 2a. The small standard deviation within these samples (n = 5 for each mixing ratio tested) indicates good repeatability even though the nanofillers are randomly distributed.

Based on the results shown in Fig. 2a, under 1 MPa loading stress, the energy density of deformation energy, viscous dissipation energy and effective converted energy of p-NCs were calculated and plotted in Fig. 2b. The deformation energy per volume were ~1.11 MJ m^{-3}, ~0.29 MJ m^{-3} and ~0.38 MJ m^{-3} for 20 : 1, 10 : 1 and 5 : 1 p-NCs, while the viscous dissipation energy per volume were ~0.149 MJ m^{-3}, ~0.021 MJ m^{-3} and ~0.034 MJ m^{-3}, respectively. Although the viscous dissipation energy proportion of 20 : 1 p-NC is the largest (~13.5%) in the total deformation energy compared to 5 : 1 and 10 : 1 p-NC, the effective converted energy of 20 : 1 p-NC is still the largest at a given load. It is expected that the 20 : 1 p-NC would have the best piezoelectric performance among three compositions due to its best capability to transfer the mechanical energy to the piezoelectric particles, which will be beneficial for a higher energy output.

Additionally, the permittivities of the p-NCs were calculated from measured capacitance values using LCR-meter (LCR-819 from GW Instek) based on the relation $C = \varepsilon_{\text{p-NC}} \frac{A}{d}$,[46] where C is the capacitance, $\varepsilon_{\text{p-NC}}$ is the permittivity of the p-NC, A and d are the surface area and thickness of the p-NC, respectively. The permittivity of the 20 : 1, 10 : 1 and 5 : 1 p-NCs were ~3.95 × 10^{-11} F m^{-1}, ~3.26 × 10^{-11} F m^{-1} and ~3.04 × 10^{-11} F m^{-1}, respectively. The 20 : 1 p-NC with the largest portion of PDMS monomer showed the largest dielectric constant while the 5 : 1 p-NC showed the smallest one.

Next, we measured the piezoelectric output of the three different groups of p-NCs and compared the results with those from the analytical predictions under quasi-static loading conditions (see ESI S6† for the measurement details). The load is applied by directly putting a weight to the top surface of p-NCs. The accumulated charge was measured from a digital electrometer (type 616, Keithley), while the real-time charge accumulation profile was recorded by a digital oscilloscope (TDS2024B, Tektronix). Fig. 2c shows the experimental results with real-time charge accumulation and dissipation profiles for the three different groups of p-NCs during loading and unloading cycles of a 200 g applied weight. The shape of the charge profile, an immediate rise and fall of the charge in response to stress along with minimal change during the loading and unloading states, indicates that the prepared p-NCs exhibit the typical characteristics of piezoelectric materials. The accumulated charge amounts of 20 : 1, 10 : 1 and 5 : 1 p-NCs were 225.91 pC, 120.25 pC, and 142.97 pC, respectively, when the applied weight was 200 g, which is consistent with the predicted trend described in Fig. 2b.

The accumulated charge *vs.* applied weight (loading force) plot shows a linear relationship as Fig. 2d. From the plot, the piezoelectric coefficient (d_{33}) of 20 : 1, 10 : 1 and 5 : 1 p-NCs was determined to be ~125 pC N^{-1}, ~60 pC N^{-1}, and ~68 pC N^{-1}, respectively. For this testing method, the analytical calculations based on quasi-static loading condition are slightly revised due to the fact that the loading methods are different from the typical quasi-static loading, as shown by the measurement set-up (see ESI Fig. S6†). The strain was directly derived from the conversion of input mechanical energy to strain energy. In other words, the lost gravitational potential energy of the weight is equal to the strain energy: $Mg\Delta L = VU_S = VE_0\varepsilon^2/2$, where M is the applied weight, ΔL is the displacement. Consequently, the dissipation energy density was calculated

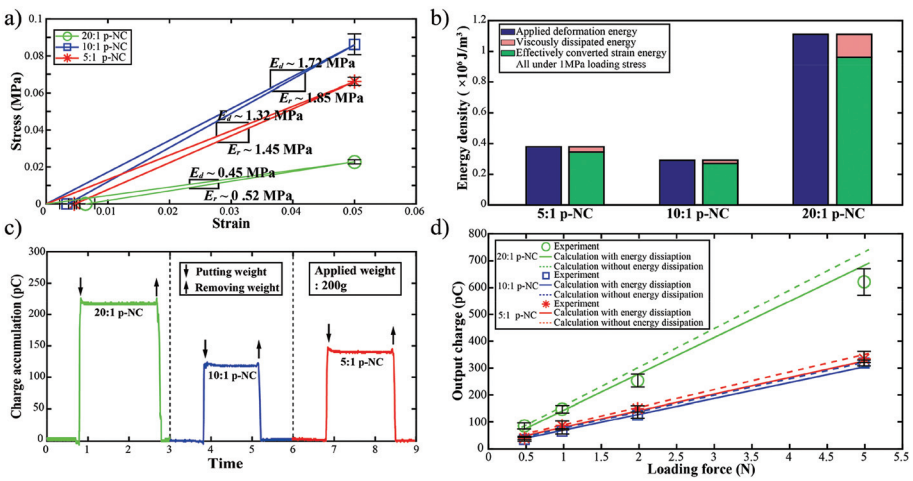

Fig. 2 Mechanical and piezoelectric responses of p-NCs. (a) The loading deformation modulus (E_d) and unloading recovery modulus (E_r) of the p-NCs at ε = 0.05(5%) under quasi-static tensile loading. (b) The energy density (under 1 MPa loading stress) of deformation energy, viscously dissipated energy and effectively converted energy of p-NCs. (c) Real-time charge accumulation and dissipation profiles for the three different groups of p-NCs during d_{33} measurements using a 200 g applied weight. (d) The charge *vs.* applied force plot for d_{33} measurements. Error bars indicate standard deviations from 5 independent measurements.

from the strain. The analytical results (solid lines in Fig. 2d) showed good agreements with experiments. The data demonstrate that p-NC with the softest matrix has the best piezoelectric performance due to the largest converted strain energy under a given loading condition (Fig. 2b). In addition, the analytical calculation without energy dissipation (dashed lines in Fig. 2d) overestimated the piezoelectric output of the p-NCs. This result demonstrates the importance of viscous effects on the piezoelectric performance of the p-NCs. Both analytical calculations and experimental results clearly indicate that the piezoelectric response is dependent on both elastic and viscous properties of the p-NCs.

For the dynamic loading conditions, the storage and loss moduli of the prepared p-NCs were measured by using dynamic mechanical analyzer (DMA, TA Instruments TA Q800) at a constant strain of 0.5%. The storage and loss moduli of the p-NCs are shown as a function of loading frequencies in Fig. 3a. When the loading frequency was between 1 and 10 Hz, both the storage and the loss moduli increased with the increase of the loading frequency. Based on the eqn (13), it is expected that the piezoelectric response will decrease with the loading frequency in this range due to the larger modulus. On the other hand, for 10 to 100 Hz loading frequency range, the storage modulus showed a valley at 50 Hz and peak at 70 Hz, while the valley and peak of the loss modulus were at 30 Hz and 70 Hz, respectively. These valleys and peaks may come from the molecular interaction among the PDMS matrix and the fillers. Based on the eqn (10) and (11), stored energy density and dissipated energy density were calculated as a function of loading frequency under 1 MPa loading stress (see ESI Fig. S7†). To decouple the influences of the dynamic loading on the electric properties, we also measured the permittivity of the p-NC (see ESI S8† for details) as a function of loading frequencies. We found that the permittivities of the p-NCs were constant for 1 to 100 Hz loading frequency range, as shown in Fig. 3b. Therefore, the changes in energy densities will consequently influence the electrical output as eqn (13). Based on the results above, we calculated analytically predicted piezoelectric constants (d'_{33}) under dynamic loading conditions as the solid/dashed lines in Fig. 4a. The plot shows the expected changes of piezoelectric performance with the loading frequency.

To verify the analytical predictions, a custom set-up was built to characterize the piezoelectric performance of the p-NCs (see ESI S9† for the set-up details) under dynamic loading conditions. A mini-shaker (type 4810, Brüel & Kjær) was used to apply cyclic loadings to the piezocomposites and the generated loading stresses were monitored by a load cell (LRM200, 10 lb, Futek). As dynamic loading force was applied by a mini-shaker, the p-NC was compressed causing a piezoelectric potential across the p-NC. The generated electrical charges were measured by a charge amplifier (piezo film lab amplifier, TE Connectivity) and an oscilloscope (TDS2024B, Tektronix). The repeated cycles of in-phase loading force signal and the output voltage signal of the 20 : 1 p-NC at 2 Hz and 10 Hz loadings are shown in Fig. S10a (ESI†). There is no offset

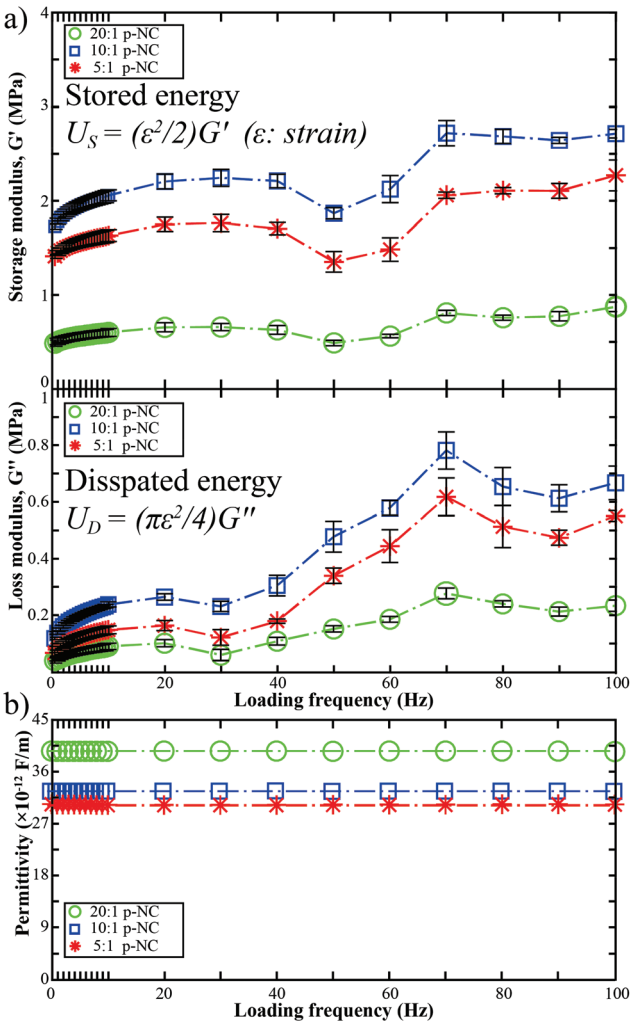

Fig. 3 Mechanical and electrical response of the p-NCs under dynamic loading condition. (a) The storage (top) and loss moduli (bottom) as a function of a loading frequency of the p-NCs. Error bars indicate standard deviations from 5 independent measurements. (b) The measured permittivity of each p-NCs as a function of a loading frequency. (All the connecting dotted lines are for visual guides.)

between the maximum voltage and maximum force. This suggests that we can precisely estimate the dynamic piezoelectric coefficients for our p-NCs from the maximum applied force and maximum output voltage.

As shown in Fig. 4a, the piezoelectric responses of p-NCs generally changed with the changing loading frequency because the mechanical response of viscoelastic materials is dependent on the loading frequency. The 20 : 1 p-NC with the smallest storage modulus showed the best piezoelectric performance, which matches with the finding from the quasi-static testing. Importantly, the predictions that considered the viscous energy dissipation (solid lines in Fig. 4a) showed good agreement with the experimental results, while those without considering the viscous energy dissipation (dashed lines in Fig. 4a) overestimated the piezoelectric outputs, especially at

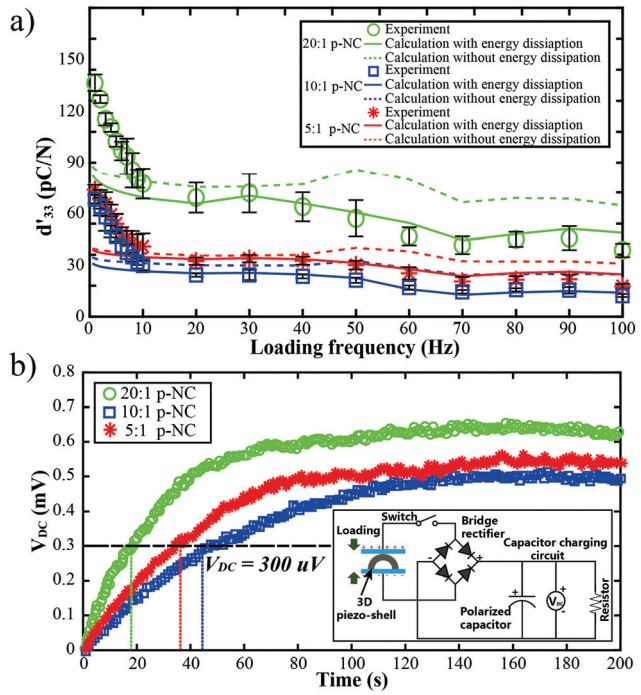

Fig. 4 Piezoelectric response of the p-NCs under dynamic loading condition. (a) The plots of dynamic piezoelectric coefficient (d'_{33}) as a function of loading frequencies at 1–100 Hz. (b) Direct-current voltages measured across a 1000 pF capacitor when it was charged by the piezo-shell made of 20 : 1, 10 : 1 and 5 : 1 p-NC under 0.5 N compression loading at 10 Hz. Inset is the equivalent charging circuit. Error bars indicate standard deviations from 5 independent measurements.

10–100 Hz loading frequency range. For example, at 50 Hz, the storage moduli of the three groups of p-NCs are the smallest, which indicate that the mechanical deformation energy can be the largest. Thus, if the viscous effects are neglected, it is expected that the piezoelectric output will be the highest at 50 Hz. However, from 30 Hz to 70 Hz, the measured dynamic piezoelectric coefficient (d'_{33}) kept decreasing because of the increase of the viscous energy losses. This result confirms that it is important to consider the loss modulus of a matrix besides the storage modulus because mechanical stress from an external loading should be efficiently transferred to the piezoelectric particles through the matrix with minimum energy dissipation. Due to the highest storage and loss moduli, the piezoelectric performances of the p-NC were the worst at 70 Hz. To be noted here is due to instrumental limitation, one single loading pulse cannot last longer than 0.1 s. This means, at low loading frequency (1–10 Hz), a single loading pulse cannot occupy a cycle time, while the system is at rest between loading pulses. However, with increase of loading frequency (>10 Hz), each single loading pulse can fully occupy its own period and the gaps are eliminated. As a result, the loading pattern is transiting from repeating single pulses (quasi-static) to continuous sine wave (dynamic), as Fig. S10a† shows. Thus, for comparison, we plotted estimations from quasi-static models *versus* the experimental results at 1–10 Hz (Fig. S10b†) as well. It clearly shows that quasi-static model works better in lower frequency, while dynamic model is better when approaching 10 Hz. Therefore, under dynamic loading conditions, the piezoelectric performances of the viscoelastic piezocomposites are dependent on the loading frequency and both the storage and loss moduli contribute to the resulting piezoelectric outputs. Thus, it is expected that the best piezoelectric response can be obtained when both the storage and loss moduli are the smallest.

As a potential application of the findings above, we fabricated flexible 3D piezo-shells made of 20 : 1 p-NC, 10 : 1 p-NC and 5 : 1 p-NC to charge a commercial capacitor, respectively. As the equivalent circuit shown in the inset of Fig. 4b, the piezo-shell was sandwiched by two flat loading plates and connected to a predesigned rectifying circuit composed of a polarized capacitor and bridge rectifier (see ESI S10† for the details). Then, it was activated by 0.5 N compressing loading at 10 Hz to conduct the capacitor charging process. The generated alternating current (AC) piezoelectric output was fully rectified through the bridge circuit and simultaneously stored in a commercial capacitor (1000 pF). The entire charging process was recorded by monitoring the converted direct-current (DC) potential across the capacitor by using a voltmeter. Fig. 4b illustrates the charging process of the capacitor with different piezo-shells. The piezo-shell made of 20 : 1 p-NC showed the highest saturation voltage of the capacitor, which is a result of equilibrium established between the piezo-shell charging rate and the capacitor's leakage rate. In addition, the 20 : 1 p-NC sample showed the fastest charging rate. The charging rate of the 20 : 1, 5 : 1 and 10 : 1 piezo-shells was ~16.7 μV s^{-1}, ~8.4 μV s^{-1} and ~6.8 μV s^{-1}, respectively. The results showed a good agreement with the analytical and experimental findings that soft piezoelectric nanocomposites (*e.g.* 20 : 1 p-NCs) with smallest elastic and viscous modulus can result in highest piezoelectric performance.

Numerical simulations

To further extend the understanding of our analytical findings by considering finite deformation of objects with complex shapes made of nonlinear materials, a multi-physics finite element (FE) model has been developed to couple transient electromagnetic and dynamic mechanical fields in the time-domain, based on the theory of electromagnetics in dynamically deforming media.[48,49] The model is implemented here to predict the evolution of electric field in the piezoelectric-viscoelastic systems subjected to dynamic loading conditions. Simulations were performed for different geometries and varying input parameters of p-NC, undergoing finite deformation under dynamic conditions. In addition to providing verifications for the aforementioned experimental studies, this robust finite element model allows us to efficiently investigate the effect of material properties on the piezoelectric performance of p-NC structures, in configurations that are challenging to achieve with experiments.

In the coupled piezoelectric computational model, a two-way coupling is established between the electric and mechanical fields in a staggered manner. At each time step, the mechanical field is first solved, and the electric field is then calculated accordingly in the updated configuration, with inputs on the displacement and velocity fields from the deformation solution. Information of the electric field is transferred back to the mechanical field in the following time step, to evaluate the reverse piezoelectric response.[48,49] The piezoelectric coupling is achieved in the reference configuration of the mechanical problem to accommodate finite deformation, as given in eqns (14) and (15):

$$D_K = E_{KIJ}E_{IJ} + \varepsilon J C_{LK}^{-1}E_L \tag{14}$$

$$S_{IJ} = S_{IJ}^{ME} + S_{IJ}^{Piezo} + S_{IJ}^{Maxwell} \tag{15}$$

where D_K is electrical displacement vector, E_{IJ} is the Green-Lagrange strain tensor, E_L is the electric field, ε is permittivity, J is Jacobian of the deformation, and E_{KIJ} is the transformed piezoelectric stress coefficient e_{mnp} in the reference configuration. The piezoelectric stress coefficient is defined as $e_{mnp} = d_{mjk}C_{jknp}$, where d_{mjk} is the piezoelectric (strain) coefficient that was studied in the experimental section and C_{jknp} is the elasticity stiffness tensor. The stress coefficient is transformed by the relation $E_{KIJ} = \frac{1}{2}JF_{Km}^{-1}e_{mnp}(F_{In}^{-1}F_{Jp}^{-1} + F_{Ip}^{-1}F_{Jn}^{-1})$. As shown in eqn (15), the second Piola-Kirchhoff stress tensor (S_{IJ}) is the sum of stress contributions from the mechanical part (S_{IJ}^{ME}), the piezoelectric part (S_{IJ}^{Piezo}), and the Maxwell stress ($S_{IJ}^{Maxwell}$), each of which is expressed as:

$$S_{IJ}^{ME} = \frac{\partial \Psi^{ME}}{\partial E_{IJ}} - Q_{IJ} \tag{16}$$

$$S_{IJ}^{Piezo} = -E_{KIJ}E_K \tag{17}$$

$$S_{IJ}^{Maxwell} = -\frac{1}{2}\varepsilon J[(E_P C_{PQ}^{-1}E_Q)C_{IJ}^{-1} - E_P E_Q(C_{PI}^{-1}C_{JQ}^{-1} + C_{PJ}^{-1}C_{IQ}^{-1})] \tag{18}$$

Here C_{IJ} is the right Cauchy-Green deformation tensor, $\Psi^{ME}(C_{IJ})$ is the stored elastic energy density, and Q_{IJ} is the non-equilibrium viscous stress. The evolution of Q_{IJ} is specified by a rate equation describing the viscoelastic material model;[41,50]

$$\dot{Q}_{IJ} + \frac{1}{\tau}Q_{IJ} = \frac{(1-\gamma)}{\tau}\mathrm{dev}\left[\frac{\partial \bar{\Psi}}{\partial \bar{E}_{IJ}}\right] \tag{19}$$

where $\tau \in (0,\infty)$ is relaxation time, $\gamma \in (0,1)$ is a given parameter, $\bar{\Psi}$ is the deviatoric part of Ψ^{ME}, and $\bar{E}_{IJ}$ is the volume-preserving part of the strain tensor E_{IJ}.

We first simulate uniaxial cyclic compression tests of the 20 : 1, 10 : 1 and 5 : 1 p-NCs and compare the steady-state peak output surface charge density with the experimental measurements, discussed earlier. Recall that the piezoelectric coefficient at a given loading frequency is a function of the storage and loss moduli. At each loading frequency, the input piezoelectric coefficient of the material is determined according to the analytical model of eqn (13), from the measured values of storage and loss moduli shown in Fig. 3. In the FE model, viscoelastic behavior of a material is described by a pair of mechanical parameters, *viz.* the instantaneous modulus (G_0) and viscous relaxation term (μ_0). The parameters are calibrated to satisfy the following two conditions:[41,50–52]

$$G_\infty = G_0(1-\mu_0) \tag{20}$$

$$G'(\omega) = G_\infty + \frac{G_0\mu_0(\omega\tau)^2}{1+(\omega\tau)^2} \tag{21}$$

where ω is the angular frequency of the applied loading, G_∞ is the equilibrium long-term elastic modulus determined by the quasi-static loading tests, and $G'(\omega)$ and τ are storage modulus and relaxation time determined by the dynamic loading tests. The 3D mesh and boundary conditions of the model are depicted in Fig. 5a. The plate is grounded at the bottom surface by setting its electric potential to φ = 0 and uniform cyclic compression load is applied on the top surface, with a traction magnitude given as:

$$T(t) = \frac{T_p}{2}[1 + \sin\left(\omega t - \frac{\pi}{2}\right)] \tag{22}$$

where T_p is the maximum prescribed compression in the cyclic loading process. This is set to be T_p = 400 Pa to match the magnitude of the load in the cyclic loading experiments.

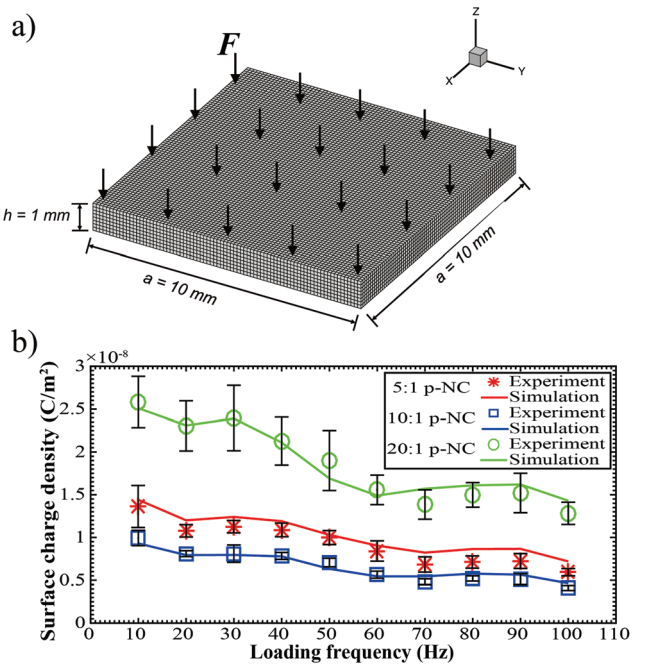

Fig. 5 Validation of simulation results by comparing with experimental results for p-NC specimens. (a) 3D model and mesh of the flat plate subjected to a cyclic compressive loading. (b) Comparison between experimental measurements and simulated results for the peak surface charge density at steady-state of loading with different frequencies, on top surface of the flat plate. Error bars indicate standard deviations from 5 independent measurements.

Difference of electric potential ($\Delta\varphi$) across the thickness of the plate is monitored, and peak value at steady-state, $\Delta\varphi_p(T_p,\omega)$, is recorded to compute the peak surface charge density $\rho_p(T_p,\omega)$ according to the eqn (23), stated as:

$$\rho_p(T_p,\omega) = \frac{\varepsilon_r\varepsilon_0}{d}\Delta\varphi_p(T_p,\omega) \quad (23)$$

where d is the plate thickness, $\varepsilon_0 = 8.85 \times 10^{-12}$ F m^{-1} is the permittivity in vacuum, and ε_r is the relative permittivity of the material. The FE predictions of $\rho_p(T_p,\omega)$ are compared with experimental results in Fig. 5b. The FE model with the calibrated material parameters is able to capture the piezoelectric behavior in the p-NCs under uniaxial cyclic compression and reproduce the relation between loading frequency and peak steady-state charge output.

A major advantage of the p-NC is its accommodation of large deformation. Hence, it is of great interest to investigate the piezoelectric performance of the material under dynamic, finite deformation conditions. To accomplish this, we simulate uniaxial cyclic tension and compression of the 20 : 1 p-NC (quasi-static modulus $E_\infty = 450$ kPa) at a frequency of 10 Hz. In addition to examining the effect of finite deformation, the dependence of piezoelectric output on the direction of applied loading is characterized by studying both tensile and compressive cyclic loading conditions. Here, we apply peak loading values of $T_p = \pm1$ kPa, ±10 kPa, and ±100 kPa, with the loading pattern described by eqn (22). Additionally, we investigate the effect of material incompressibility on the piezoelectric performance. The original material model is nearly-incompressible, with Poisson's ratio set to $\nu = 0.499$. We perform the same set of simulations on a modified material model with Poisson's ratio of $\nu = 0.30$ and other input parameters, G_0, $\mu_0(\omega)$, τ, $d_{33}(\omega)$, and ε_r, assumed to be unchanged. In the real p-NC materials, it is challenging to adjust the Poisson's ratio without changing the other properties. However, the computational models allow for decoupling of these input parameters. The time histories of the surface charge density are shown in Fig. 6a–c, and the measured peak magnitudes of surface charge density in the aforementioned cases are shown in Fig. 6d.

We observe that a higher output charge density is produced for cyclic tension than for cyclic compression with equal magnitude of peak load $|T_p|$. The advantage of applying cyclic tension is more profound when $|T_p|$ is high and the material is nearly incompressible. For the compressible material model ($\nu = 0.30$), the electric fields generated under cyclic tension and compression are in opposite directions, which can be noticed from the time history of output charge in Fig. 6a–c. However, this is not the case for the nearly incompressible material model ($\nu = 0.499$). When the nearly incompressible material is subjected to cyclic compression of relatively large peak load, the piezoelectric field is in the same direction as

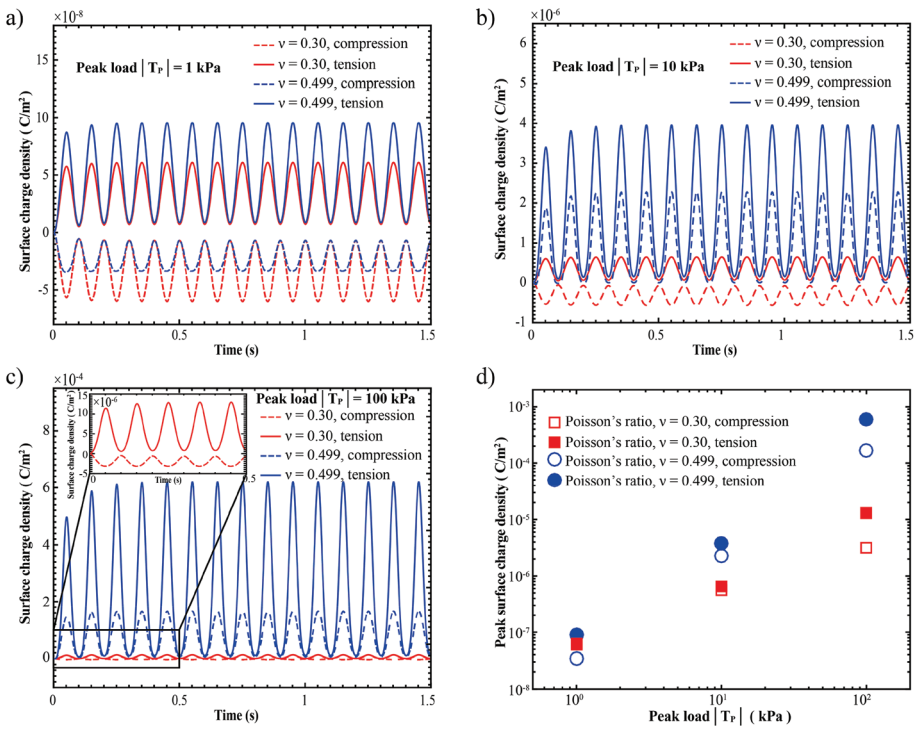

Fig. 6 (a)–(c) The comparison of surface charge density time history under compressive and tensile cyclic loadings for models with different Poisson's ratios ($\nu = 0.30$ and 0.499, respectively). (a) Peak load $|T_p| = 1$ kPa; (b) $|T_p| = 10$ kPa; (c) $|T_p| = 100$ kPa. For the compressible material model, the output signals under large cyclic tensile and compressive loading are in opposite directions. The inset in c is the magnified view. (d) Peak magnitude of the surface charge density for compressible (Poisson's ratio $\nu = 0.30$) and nearly-incompressible (Poisson's ratio $\nu = 0.499$) models of 20 : 1 p-NC under large cyclic deformation.

that generated by cyclic tension. This can be explained by the earlier discussion on piezoelectric fields in incompressible material under large deformation. Since the Poisson's ratio is slightly below 0.5 for the nearly incompressible case studied here, the piezoelectric coefficient e_{33} is slightly larger than e_{31} and e_{32}. As a result, when the material is subjected to a small amount of uniaxial compression, the contribution of E_{33} to the electric field is still stronger than the total contribution due to E_{11} and E_{22}, as observed in Fig. 6a. When the material is further deformed, the generated electric field switches direction, as seen in Fig. 6b and c. This suggests that, by adjusting the Poisson's ratio of the p-NC material, we can control the possible direction of the piezoelectric field generated under large deformation conditions.

To further verify the robustness of the calibrated FE model, we simulate the dynamic loading tests of flexible 3D piezo-shells as shown in Fig. 7. It is worthwhile to note that in this configuration, the piezoelectric material is poled along the radial direction of the curved shell structure, and the plate is grounded across its inner surface, *i.e.* $\varphi(r = r_i) = 0$. Since the piezoelectric coupling is performed in the reference configuration, update of the piezoelectric constant tensor is not necessary during the finite deformation simulations. Due to displacements of the deformed structure, the electric potential field is non-uniform along the outer surface of the shell. An example of typical distribution is shown in Fig. 7a. In this case, we

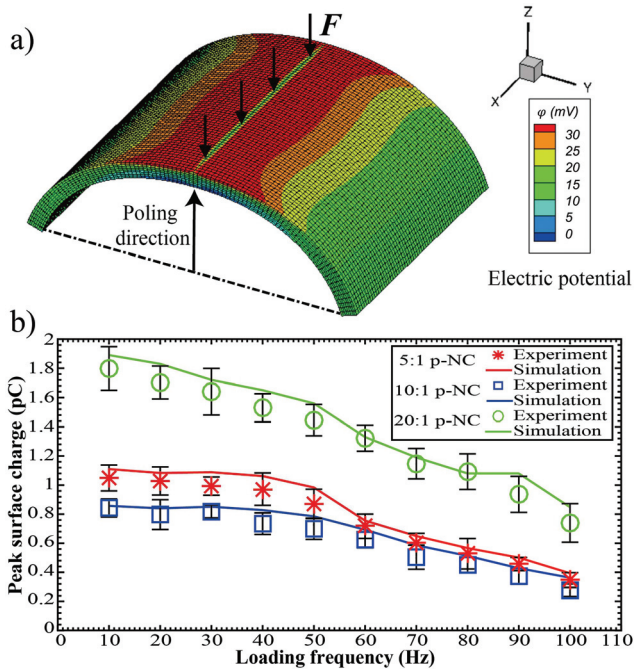

Fig. 7 (a) Electric potential distribution in the 3D model of a p-NC shell structure subjected to cyclic compression, poled along radial direction and grounded across inner surface. (b) Comparison of measured *vs.* computed peak total surface charges with different frequencies, across the top surface of the curved shell. Error bars indicate standard deviations from 5 independent measurements.

compare the peak total surface charge (Q_p) across the shell surface from the relation

$$Q_p(P_p, \omega) = \frac{\varepsilon_r \varepsilon_0}{d} \int_{A_s} \Delta\varphi_p(P_p, \omega, \boldsymbol{x}) dA \tag{24}$$

where P_p is the peak compressive load applied, $\boldsymbol{x}$ is the coordinate of the point studied on the shell surface, $\Delta\varphi_p$ is the peak difference of electric potential measured across the shell thickness, and A_s is the surface of the shell structure. As shown in Fig. 7b, the simulation results are generally in good agreement with the experimental measurements. The numerical predictions are slightly higher than the experimental measurements. This may be attributed to some uncertainties in the fabrication process of the piezo-shell specimens and/or charge leaking during measurements.

To provide additional guidance to the design of p-NCs, a sensitivity study is conducted with the FE model to help seek an optimal set of mechanical parameters for high piezoelectric performance. We investigated the effects of each of the three input mechanical parameters, *viz.* the instantaneous modulus (G_0), viscous relaxation (μ_0), and relaxation time (τ), on the peak charge output in a cyclically loaded p-NC plate polarized in the loading direction shown in Fig. 5a. For a given set of (G_0,μ_0,τ), we may determine the storage modulus at an assigned loading frequency according to eqn (21). Then, we utilize the available data of experimentally measured pairs of storage and loss moduli in the synthesized p-NC specimens to interpolate the corresponding loss modulus (G'') for a given storage modulus (G'). Experimental results discussed earlier, confirm that permittivity is not significantly altered by the adjustment of the mechanical parameters in the polymeric matrix. From eqn (13), we can calculate the piezoelectric constant $d_{33}(G',G'')$ as we adjust the parameters (G_0,μ_0,τ), while maintaining a constant value of piezo-particle volume ratio in the composite. In the sensitivity study, the loading condition is set to be uniaxial cyclic compression at 10 Hz, with pattern described by eqn (22) and maximum load T_p was set to 400 Pa.

Fig. 8 shows the change in time history of surface charge density, when we adjust G_0, μ_0, and τ, respectively, while keeping other mechanical input parameters constant. As shown in the Fig. 8a, when the overall stiffness of the p-NC material is decreased, an increase in piezoelectric output is observed. This agrees with the experimental observations discussed earlier. In the load-control setting examined here, this is due to the overall increase of piezoelectric constant $d_{33}(G', G'')$ when G' decreases significantly. To examine this phenomenon, we can rewrite the eqn (13) as:

$$\begin{aligned} d_{33} &= \varepsilon_{\text{p-NC}} \sqrt{\frac{2V_{\text{piezo}}}{\varepsilon_{\text{piezo}} V}} \cdot \sqrt{\frac{\frac{1}{2}G' - \frac{\pi}{4}G''}{G'^2 + G''^2}} \\ &= \varepsilon_{\text{p-NC}} \sqrt{\frac{2V_{\text{piezo}}}{\varepsilon_{\text{piezo}} V}} \cdot A(G', G'') \end{aligned} \tag{25}$$

where the change of viscoelastic contribution factor $A(G',G'')$ following the adjustment of G' and G'' dictates the change of

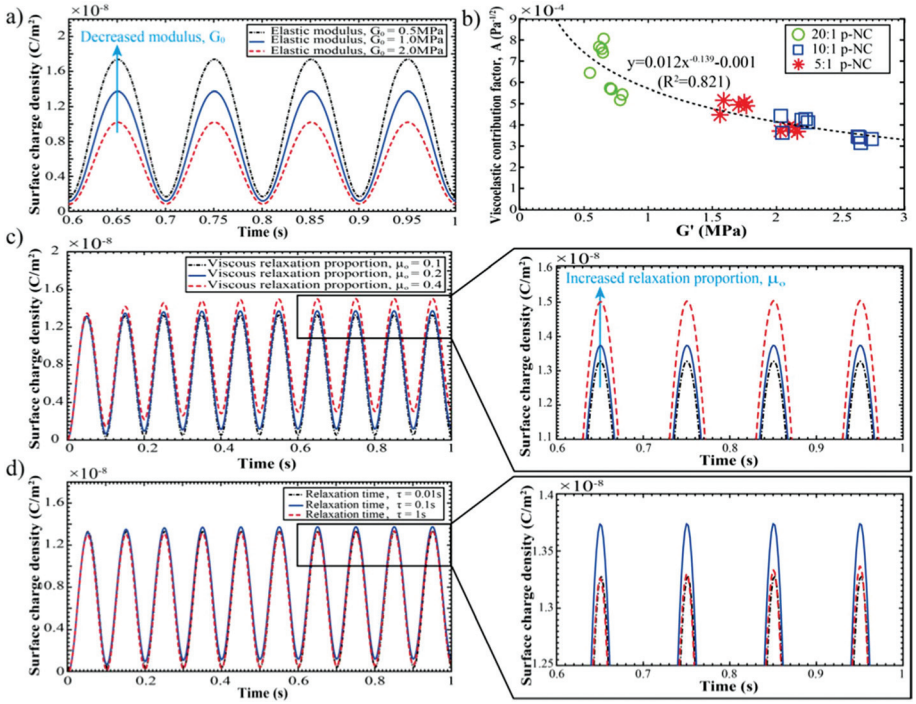

Fig. 8 Parametric studies showing effects of controlling viscoelastic properties of p-NC. (a) Comparisons of time history of the surface charge density for p-NC models with different instantaneous elastic modulus (G_0). (b) Dependence of viscoelastic contribution factor $A(G',G'')$ on storage modulus (G'), based on experimental measurements. (c) Comparison of time history of the surface charge density for p-NC models with different viscous relaxation proportion (μ_0). (d) Comparison of time history of the surface charge density for p-NC models with different relaxation time (τ).

piezoelectric performance. For the experimentally measured pairs of (G',G''), the corresponding values of $A(G',G'')$ is shown in Fig. 8b, with $A(G',G'')$ displaying a decreasing trend when G' is increased. This sheds light on why a higher piezoelectric output is observed in the softer p-NC specimens and that a lower overall modulus is desired in this class of material because the piezoelectric output is proportional to $A(G',G'')$ as in eqn (25).

The effect of material relaxation on the piezoelectric output can be examined from the results shown in Fig. 8c. When one-way cyclic loading is applied to the viscoelastic material, relaxation in elastic modulus leads to residual stress when the material is fully unloaded, which is converted to residual surface charge in the viscoelastic-piezoelectric system. The buildup of residual charge after each loading cycle leads to the gradual increase of peak surface charge, until the system finally reaches an equilibrium state. This phenomenon can be observed from Fig. 8c that a higher viscous relaxation (μ_0) allows for a more relaxation in the material, and therefore a greater increase of peak surface charge after multiple cycles of one-way loading. This suggests that for applications where one-way dynamic loading is anticipated, an increased amount of viscous relaxation is beneficial for higher piezoelectric peak output.

Fig. 8d shows the effect of relaxation time (τ) on the time history of surface charge density. In this case, given an applied loading frequency of 10 Hz and constant G_0 and μ_0 in the material model, a moderate relaxation time (τ = 0.1 s) produces higher steady-state peak surface charge than those with much shorter (τ = 0.01 s) or much longer relaxation time (τ = 1 s). This can be explained by the fact that viscoelastic solids respond to loadings in an elastic manner, when undergoing very fast or very slow processes.[52–54] When the loading cycle is very long relative to the relaxation time, the viscoelastic material behaves effectively as a softened elastic solid and minimal residual stress is accumulated during the loading-unloading process. When the loading cycle is very short relative to the relaxation time, there is insufficient time for a considerable amount of viscous energy dissipation to occur, and therefore the viscoelastic material behaves effectively as a stiff elastic solid. In other words, when the ratio of loading cycle length to relaxation time is too low or too high, mechanical behavior of the material converges towards elasticity, and, consequentially, we can effectively reduce the influence of viscous energy dissipation. To increase the conversion of applied mechanical energy to electric energy, it is thus beneficial for the material's relaxation time to be much shorter or much longer relative to the length of the applied loading cycle.

Conclusion

We investigated the viscoelastic effects on piezoelectric performance of soft piezocomposites theoretically and experi-

mentally under both quasi-static and dynamic loading conditions. Our predictions from analytical and numerical models showed good quantitative match with experimental results. Our results show that not only elastic characteristics, but also viscous properties play important roles in the piezoelectric performance of piezoelectric polymer composites with viscoelastic matrix. Under quasi-static loading conditions, the piezoelectric coefficient (d_{33}) of the specimen with the lowest Young's modulus (~0.45 MPa at 5% strain) was ~120 pC N^{-1}, while the one with the highest Young's modulus (~1.3 MPa at 5% strain) was ~62 pC N^{-1}. Softer matrices with small elastic modulus enhance the energy harvesting performance because they can result in larger deformation for a given load. On the other hand, piezoelectric responses from the p-NCs are dependent on the loss (viscous) modulus as well as the storage (elastic) modulus, due to the fact that part of the total work of mechanical deformation energy input is dissipated as heat through viscous loss which reduces the resulting piezoelectric outputs. Under dynamic loading conditions, the storage moduli (G') of the softest specimen were ~0.625 MPa and ~0.485 MPa at 40 Hz and 50 Hz, while the loss moduli (G'') were ~0.108 MPa and ~0.151 MPa, respectively. As piezocomposites with less viscous loss can transfer mechanical energy more efficiently to piezoelectric particles, the dynamic piezoelectric coefficient (d_{33}) measured at 40 Hz (~53 pC N^{-1}) was larger than that at 50 Hz (~47 pC N^{-1}) though it has a larger storage modulus. From our study, soft piezoelectric nanocomposites with the smallest elastic and viscous moduli resulted in the highest piezoelectric performance. To demonstrate the practical implication of the p-NCs with varied viscoelastic properties, we fabricated flexible 3D piezo-shells with different viscoelastic properties and compared the charging time. The charging rate of the 20 : 1 ($G' \sim 0.7$ MPa, $G'' \sim 0.1$ MPa at 10 Hz), 5 : 1 ($G' \sim 1.7$ MPa, $G'' \sim 0.15$ MPa at 10 Hz), and 10 : 1 ($G' \sim 2$ MPa, $G'' \sim 0.23$ MPa at 10 Hz) piezo-shells was ~16.7 μV s^{-1}, ~8.4 μV s^{-1} and ~6.8 μV s^{-1}, respectively. The results showed a good agreement with the predicted trend from theoretical and experimental studies that the composition with the smallest elastic and viscous modulus showed the fastest charging rate.

To further extend the understanding of our analytical findings by considering finite deformation of objects with complex shapes made of nonlinear materials, a multi-physics finite element model has been developed to couple transient electromagnetic and dynamic mechanical fields in the time-domain, based on the theory of electromagnetics in dynamically deforming media. Numerical models were first calibrated by incorporating experimentally measured mechanical properties and analytical prediction of piezoelectric constant into a multi-physics finite element framework. Then, we conducted sensitivity studies using our numerical model to investigate the relations between input parameters of the p-NC model and the piezoelectric output to provide guidance for a desired set of mechanical properties in the studied configuration. In particular, we investigated the effects of the Poisson's ratio and the relaxation time. We found that while the electric fields generated under cyclic tension and compression are in opposite directions for the compressible material model ($\nu = 0.30$), they were in the same direction for the nearly-incompressible material model ($\nu = 0.499$). Moreover, we found that it is beneficial for the material's relaxation time to be much shorter or much longer relative to the length of the applied loading cycle to increase the conversion of applied mechanical energy to electric energy. When the ratio of loading cycle length to relaxation time is too low or too high, mechanical behavior of the material converges towards elasticity, and, consequentially, we can effectively reduce the influence of viscous energy dissipation.

Overall, both our theoretical and experimental results have demonstrated the significant effects of viscoelasticity on electromechanical behavior of p-NC. Based on the analytical studies and the numerical simulations, we can further enhance the energy harvesting performance of soft energy harvesters and sensitivity of flexible sensors by harnessing the viscoelasticity of piezocomposites. Our findings are not only applicable to piezoelectric composites, but also open new opportunities for optimizing the capabilities of polymer-based (multi-)functional materials by harnessing the viscoelastic properties.

Experimental section

Synthesis of the p-NC

(1) The carbon nanotubes (CNTs) and $BaTiO_3$ nanoparticles (BTO NPs) were first dispersed in absolute ethyl alcohol (ACS reagent, ≥99.5%, Sigma Aldrich) by magnetic stirring for 5 hours and ultrasonication for 60 minutes and were subsequently mixed with the PDMS monomer (Sylgard 184 available from Dow Chemical) using revolutionary mixer (KK-400W, Mazerustar) for 270 seconds. (2) The mixture was placed in an oven (Lindberg/Blue M™ vacuum ovens, Thermo Scientific™) at 70 °C until the alcohol completely evaporated. Then, the PDMS curing agent was added to the mixture, which was then uniformly dispersed using revolutionary mixer (KK-400W, Mazerustar) for 180 seconds. The mass ratio between the PDMS monomer and curing agent was adjusted to control the mechanical properties. (3) The uncured BTO/CNTs/PDMS composite was poured to the mold and degassed in a vacuum chamber (Economy vacuum chambers system, A-VAC Industries). (4) The mixture was then cured in an oven at 120 °C for 20 minutes. Subsequently, the solidified p-NC was put at the room temperature for 24 hours to ensure that the p-NC was completely cured. The synthesized p-NC could be cut into any shape and size according to experimental requirements.

Piezoelectric coefficient (d_{33}) measurement

The in-house built piezoelectric coefficient measurement systems are shown in ESI, S6 and S9,† respectively. For determining the piezoelectricity coefficient (d_{33}), the p-NC with Au/Cr electrodes (thickness ~200 nm) was sandwiched between two insulated plates. The bottom side plate was fixed

and the loading force was applied by putting different calibration weights (available from Magikon). The generated charges were measured by an electrometer (616 digital Electrometer, Keithley) and an oscilloscope (TDS2024B, Tektronix). For determining the dynamic piezoelectricity coefficient (d'_{33}), the p-NC with Au/Cr electrodes was sandwiched between two insulated plates. One plate was attached to the mini-shaker (type 4810, Brüel & Kjær) while the other was connected to the load cell (LRM200, 10 lb, Futek) fixed to the support frame. The mini-shaker was driven by a synthesized function generator (DS345, Stanford Research) and a piezo amplifier (EPA104, Piezo Systems). The loading stress was measured by the load cell. The charge generated during the dynamic compression stress was measured by a charge amplifier (Piezo Film Lab Amplifier, TE Connectivity) and an oscilloscope (TDS2024B, Tektronix).

Conflicts of interest

There are no conflicts to declare.

Acknowledgements

This work was partially supported by the start-up fund from the Whiting School of Engineering at Johns Hopkins University (L. Fang and S. H. Kang) and the scholarship by China Scholarship Council (CSC) (J. Li). Z. Zhu, S. Guo and S. Ghosh have been supported by the Mechanics of Multifunctional Materials and Microsystems Program of the Air Force Office of Scientific Research through a Grant FA9550-14-1-0125 (program director Dr B. L. "(Les)" Lee).

References

1 J. A. Paradiso and T. Starner, *IEEE Pervasive Comput.*, 2005, **4**, 18.
2 F. D. O. Falca, *Renewable Sustainable Energy Rev.*, 2010, **14**, 899.
3 G. M. J. Herbert, S. Iniyan, S. Sreevalsan and S. Raja Pandian, *Renewable Sustainable Energy Rev.*, 2007, **11**, 1117.
4 S. Mekhilef, R. Saidur and A. Safari, *Renewable Sustainable Energy Rev.*, 2011, **15**, 1777.
5 F. R. Fan, W. Tang and Z. L. Wang, *Adv. Mater.*, 2016, **28**, 4283.
6 Z. L. Wang, G. Zhu, Y. Yang, S. Wang and C. Pan, *Mater. Today*, 2012, **15**, 532.
7 K.-I. Park, C. K. Jeong, N. K. Kim and K. J. Lee, *Nano Convergence*, 2016, **3**, 12.
8 Z. L. Wang and J. H. Song, *Science*, 2006, **312**, 242.
9 L. Persano, C. Dagdeviren, Y. Su, Y. Zhang, S. Girardo, D. Pisignano, Y. Huang and J. A. Rogers, *Nat. Commun.*, 2013, **4**, 1633.
10 G. T. Hwang, H. Park, J. H. Lee, S. Oh, K.-I. Park, M. Byun, H. Park, G. Ahn, C. K. Jeong, K. No, H. Kwon, S. G. Lee, B. Joung and K. J. Lee, *Adv. Mater.*, 2014, **26**, 4880.
11 P. K. Yang, L. Lin, F. Yi, X. Li, K. C. Pradel, Y. Zi, C.-I. Wu, J. H. He, Y. Zhang and Z. L. Wang, *Adv. Mater.*, 2015, **27**, 3817.
12 X. Xiao, L. Yuan, J. Zhong, T. Ding, Y. Liu, Z. Cai, Y. Rong, H. Han, J. Zhou and Z. L. Wang, *Adv. Mater.*, 2011, **23**, 5440.
13 S. Orrego, K. Shoele, A. Ruasa, K. Dorana, B. Caggianoa, R. Mittala and S. H. Kang, *Appl. Energy*, 2017, **194**, 212.
14 S. Lee, S. H. Bae, L. Lin, Y. Yang, C. Park, S. W. Kim, S. N. Cha, H. Kim, Y. J. Park and Z. L. Wang, *Adv. Funct. Mater.*, 2013, **23**, 2445.
15 R. Yang, Y. Qin, C. Li, G. Zhu and Z. L. Wang, *Nano Lett.*, 2009, **9**, 1201.
16 G. Zhu, R. Yang, S. Wang and Z. L. Wang, *Nano Lett.*, 2010, **10**, 3151.
17 C. Chang, V. H. Tran, J. Wang, Y. Fuh and L. Lin, *Nano Lett.*, 2010, **10**, 726.
18 M. Lee, C. Y. Chen, S. Wang, S. N. Cha, Y. J. Park, J. M. Kim, L.-J. Chou and Z. L. Wang, *Adv. Mater.*, 2012, **24**, 1759.
19 Y. Qi, N. T. Jafferis, K. Lyons Jr., C. M. Lee, H. Ahmad and M. C. McAlpine, *Nano Lett.*, 2010, **10**, 524.
20 Y. Qi, J. Kim, T. D. Nguyen, B. Lisko, P. K. Purohit and M. C. McAlpine, *Nano Lett.*, 2011, **11**, 1331.
21 K.-I. Park, S. Xu, Y. Liu, G. T. Hwang, S. J. L. Kang, Z. L. Wang and K. J. Lee, *Nano Lett.*, 2010, **10**, 4939.
22 K.-I. Park, M. Lee, Y. Liu, S. Moon, G. T. Hwang, G. Zhu, J. E. Kim, S. O. Kim, D. K. Kim, Z. L. Wang and K. J. Lee, *Adv. Mater.*, 2012, **24**, 2999.
23 K. Yang, X. Huang, Y. Huang, L. Xie and P. Jiang, *Chem. Mater.*, 2013, **25**, 2327.
24 S. H. Shin, Y. H. Kim, M. H. Lee, J. Y. Jung and J. Nah, *ACS Nano*, 2014, **8**, 2766.
25 N. Thambi and A. M. Sastry, *Smart Mater. Struct.*, 2014, **23**, 033001.
26 C. K. Jeong, K.-I. Park, J. Ryu, G. T. Hwang and K. J. Lee, *Adv. Funct. Mater.*, 2014, **24**, 2620.
27 Y. C. Mao, P. Zhao, G. McConohy, H. Yang, Y. X. Tong and X. D. Wang, *Adv. Energy Mater.*, 2014, **4**, 1301624.
28 H. Sun, H. Tian, Y. Yang, D. Xie, Y. C. Zhang, X. Liu, S. Ma, H. M. Zhao and T. L. Ren, *Nanoscale*, 2013, **5**, 6117.
29 I. Babu and G. de With, *Compos. Sci. Technol.*, 2014, **91**, 91.
30 H. M. Ning, N. Hu, T. Kamata, J. H. Qiu, X. Han, L. M. Zhou, C. Chang, Y. Liu, L. K. Wu, J. H. Qiu, H. L. Ji, W. X. Wang, Y. Zemba, S. Atobe, Y. Li, Alamusi and H. Fukunaga, *Smart Mater. Struct.*, 2013, **22**, 065011.
31 L. F. Chen, Y. P. Hong, X. J. Chen, Q. L. Wu, Q. J. Huang and X. T. Luo, *J. Mater. Sci.*, 2004, **39**, 2997.
32 V. Goodarzi and M. R. Saeb, *J. Intell. Mater. Syst. Struct.*, 2016, **27**, 2395.
33 W. R. McCall, K. Kim, C. Heath, G. La Pierre and D. J. Sirbuly, *ACS Appl. Mater. Interfaces*, 2014, **6**, 19504.

34 S. Mamada, N. Yaguchi, M. Hansaka, M. Yamato and H. Yoshida, *J. Appl. Polym. Sci.*, 2015, **132**, 41817.
35 D. Halliday, R. Resnick and J. Walker, *"Electric Potential" Fundamentals of Physics*, John Wiley & Sons, 5th edn, 1997.
36 T. Ikeda, *Piezoelectricity*, Oxford University Press, 1990.
37 W. R. Smythe, *Static and Dynamic Electricity*, McGraw-Hill, 1950.
38 M. A. Meyers and K. K. Chawla, *Mechanical behavior of materials*, Cambridge University Press, 2009.
39 N. W. Tschoegl, *The phenomenological theory of linear viscoelastic behavior: an introduction*, Springer, 2012.
40 N. G. McCrum, C. P. Buckley and C. B. Bucknall, *Principles of polymer engineering*, Oxford University Press, 1997.
41 O. C. Zienkiewicz and R. L. Taylor, *The finite element method: solid mechanics*, Butterworth-Heinemann, 2000, vol. 2.
42 J. E. Marsden and T. J. Hughes, *Mathematical foundations of elasticity*, Courier Corporation, 1994.
43 A. G. Holzapfel, *Nonlinear Solid Mechanics II*, John Wiley & Sons, 2000.
44 K. Khanafer, A. Duprey, M. Schlicht and R. Berguer, *Biomed. Microdevices*, 2009, **11**, 503.
45 R. Seghir and S. Arscott, *Sens. Actuators, A*, 2015, **230**, 33.
46 R. Calio, U. B. Rongala, D. Camboni, M. Milazzo, C. Stefanini, G. de Petris and C. M. Oddo, *Sensors*, 2014, **14**, 4755.
47 A. M. Stricher, R. G. Rinaldi, C. Barrès, F. Ganachaud and L. Chazeau, *RSC Adv.*, 2015, **5**, 53713.
48 S. Guo and S. Ghosh, *Comput. Mech.*, 2014, **54**, 407.
49 R. Yaghmaie, S. Guo and S. Ghosh, *Comput. Methods Appl. Mech. Eng.*, 2016, **303**, 341.
50 J. C. Simo, *Comput. Methods Appl. Mech. Eng.*, 1987, **60**, 153.
51 C. Zener, *Elasticity and anelasticity of metals*, University of Chicago Press, 1948.
52 R. S. Lakes, *Viscoelastic materials*, Cambridge University Press, 2009.
53 J. D. Ferry, *Viscoelastic properties of polymers*, John Wiley & Sons, 1980.
54 R. Christensen, *Theory of viscoelasticity: an introduction*, Elsevier, 2012.

